

1 **Title**

2 **Deep learning redesign of PETase for practical PET degrading applications**

3

4 Hongyuan Lu,[†] Daniel J. Diaz,[‡] Natalie J. Czarnecki,[†] Congzhi Zhu,[†] Wantae Kim,[†] Raghav Shroff,[§] Daniel J.
5 Acosta,^{†,§} Brad Alexander[§], Hannah Cole,^{†,§} Yan Jessie Zhang,[§] Nathaniel Lynd,[†] Andrew D. Ellington,[§] Hal S.
6 Alper ^{†,*}

7

8 **Affiliations**

9 [†]McKetta Department of Chemical Engineering, The University of Texas at Austin, Austin, Texas 78712, United States

10 [‡]Department of Chemistry, The University of Texas at Austin, Austin, Texas 78712, United States

11 [§]Department of Molecular Biosciences, The University of Texas at Austin, Austin, Texas 78712, United States

12 *Corresponding Author: McKetta Department of Chemical Engineering, The University of Texas at Austin, 200 East Dean Keeton St.,
13 C0400, Austin, Texas 78712, halper@che.utexas.edu

14 **Abstract**

15 Plastic waste poses an ecological challenge¹. While current plastic waste management largely relies
16 on unsustainable, energy-intensive, or even hazardous physicochemical and mechanical processes,
17 enzymatic degradation offers a green and sustainable route for plastic waste recycling². Poly(ethylene
18 terephthalate) (PET) has been extensively used in packaging and for the manufacture of fabrics and
19 single-used containers, accounting for 12% of global solid waste³. The practical application of PET
20 hydrolases has been hampered by their lack of robustness and the requirement for high processing
21 temperatures. Here, we use a structure-based, deep learning algorithm to engineer an extremely robust
22 and highly active PET hydrolase. Our best resulting mutant (FAST-PETase: Functional, Active, Stable,
23 and Tolerant PETase) exhibits superior PET-hydrolytic activity relative to both wild-type and
24 engineered alternatives, (including a leaf-branch compost cutinase and its mutant⁴) and possesses
25 enhanced thermostability and pH tolerance. We demonstrate that whole, untreated, post-consumer PET
26 from 51 different plastic products can all be completely degraded by FAST-PETase within one week,
27 and in as little as 24 hours at 50 °C. Finally, we demonstrate two paths for closed-loop PET recycling
28 and valorization. First, we re-synthesize virgin PET from the monomers recovered after enzymatic
29 depolymerization. Second, we enable *in situ* microbially-enabled valorization using a *Pseudomonas*
30 strain together with FAST-PETase to degrade PET and utilize the evolved monomers as a carbon
31 source for growth and polyhydroxyalkanoate production. Collectively, our results demonstrate the
32 substantial improvements enabled by deep learning and a viable route for enzymatic plastic recycling
33 at the industrial scale.

34 **Manuscript Text**

35 Poly(ethylene terephthalate) (PET) composes 70% of synthetic textile fibers and 10% of non-
36 fiber plastic packaging¹, and correspondingly represents an enormous waste stream of single-use,
37 manufactured materials. Yet, a circular carbon economy for PET is theoretically attainable through
38 rapid enzymatic depolymerization followed by either chemical repolymerization or microbial
39 upcycling/valorization into other products^{5,6}. However, all existing PET-hydrolyzing enzymes (PHEs)
40 are limited in their capacity to either function within moderate pH/temperature ranges or directly utilize
41 untreated post-consumer plastics. Such traits are essential for *in situ* depolymerization and for
42 simplified, low-cost industrial-scale processes⁷. To overcome these limitations, we employed deep
43 learning and protein engineering approaches to generate a PHE that has exceptionally high activity
44 across a broad range of raw PET substrates (both model and actual post-consumer PET (pc-PET)),
45 temperatures, and pH levels in a manner that out-performs all other known PHEs and rationally-
46 derived mutants.

47 Enzymatic depolymerization of PET was first reported in 2005 and has been nascently
48 demonstrated using 19 distinct PHEs derived from esterases, lipases, and cutinases^{2,7,8}. However, the
49 majority of these enzymes only show appreciable hydrolytic activity at high reaction temperatures (i.e.
50 at or exceeding the PET glass transition temperature of ca. 70 °C) and with highly processed substrates.
51 For example, an engineered leaf-branch compost cutinase (LCC) can degrade 90% of pretreated pc-
52 PET within 10 hours at 72 °C and a pH of 8.0⁴. Most other PHEs similarly show poor activity at
53 moderate temperatures⁹ and more neutral pH conditions¹⁰, greatly restricting *in situ* / microbially-
54 enabled degradation solutions for PET waste. This limitation is of critical concern as 40% of
55 uncollectable plastics reside in natural environments¹¹. In addition, converting untreated post-
56 consumer plastic waste at near ambient temperature would be preferable for industrial applications,
57 whereas elevated temperatures and pre-treatment increase net operating costs.

58 While the PHE from the PET-assimilating bacterium *Ideonella sakaiensis*⁹ (PETase) can
59 operate at ambient conditions, it is highly labile and loses activity even at 37 °C after 24 hours¹²,
60 thereby limiting practical applications. Nonetheless, this mesophilic enzyme has previously seen
61 attempts to enhance thermostability, robustness and function^{12–18}. The most notable engineered PETase
62 variants—ThermoPETase¹² and DuraPETase¹⁷—were created through rational protein engineering
63 and computational redesign strategies, respectively. Although the thermostability and catalytic activity
64 of these two mutants were improved^{12,17} under certain conditions, they nonetheless had overall lower
65 PET-hydrolytic activity at mild temperatures.

66 We posited that highly focused protein engineering approaches such as those described above
67 cannot take into account the evolutionary trade-off between overall stability and activity, and that a
68 neutral, structure-based, deep learning neural network might generally improve enzyme function
69 across all conditions. To this end, we employed our 3D self-supervised, convolutional neural network,
70 MutCompute¹⁹ ([Supplementary Information Fig. 1](#)) to identify stabilizing mutations. This algorithm
71 learns the local chemical microenvironments of amino acids based on training over 19,000 sequence-
72 diverse protein structures from the Protein Data Bank and can readily predict positions within a protein
73 where wild-type amino acids are not optimized for their local environments. We employed
74 MutCompute to obtain a discrete probability distribution for the structural fit of all 20 canonical amino
75 acids at every position in both wild-type PETase and ThermoPETase (crystal structures PDB: 5XJH
76 and 6IJ6) ([Supplementary Information Fig. 2](#)), essentially carrying out a comprehensive scanning
77 mutagenesis of the protein *in silico*. The predicted distributions were rendered onto the protein crystal
78 structure ([Fig. 1a](#)) to identify positions where wild-type amino acid residues were ‘less fit’ than
79 potential substitutions. Predictions were then ranked by predicted probabilities (fold-change of fit) ([Fig.](#)
80 [1b](#); [Supplementary Information Fig. 3](#)). Using a stepwise combination strategy, a total of 159 single
81 or multiple predicted mutations were generated in various PETase scaffolds. Variants exhibiting
82 improved catalytic activity (as measured by esterase activity and plastic degradation rates) and

83 thermostability (as measured by protein melting temperature (T_m)) were characterized further.
84 Amongst this set, four predicted mutations (S121E, N233K, R224Q and T140D) (Fig 1c) resulted in
85 the highest improvements, both singly and in combination, and were selected for further assembly and
86 analysis (see Additional Supplementary Discussion in Supplementary Information Fig. 4 for a further
87 discussion of the mutant down-select). Encouragingly, two substitutions (S121E and T140D) were
88 reported in the literature after our initial predictions, whereas the remaining residues are entirely unique,
89 thus emphasizing the importance of a neutral, deep learning-based approach to identifying critical
90 substitutions.

91 We assembled all 29 possible combinations using these four mutations across three PETase
92 scaffolds (wild-type PETase, ThermoPETase, and DuraPETase). Of note, two could not be purified
93 using the DuraPETase background after multiple attempts. Thermostability analysis of the remaining
94 27 mutants indicated that 24 (ca. 89%) resulted in elevated T_m relative to their respective scaffolds
95 (Supplementary Information Fig. 5). The highest change in thermostability from their respective
96 PETase scaffolds were observed for variants PETase^{N233K/T140D} with a T_m of 58.1 °C ($\Delta T_m=10$ °C from
97 WT PETase), ThermoPETase^{N233K/R224Q} with a T_m of 67.4 °C ($\Delta T_m=9$ °C from ThermoPETase), and
98 DuraPETase^{N233K} with a T_m of 83.5 °C ($\Delta T_m=5$ °C from DuraPETase). The latter mutant represents the
99 most thermostable PETase mutant reported to date. It was noted that the protein yield of all 27 variants
100 was improved (up to 3.8-fold increase) compared with the parental scaffold, further underscoring the
101 ability of Mutcompute to identify mutants of higher stability (Supplementary Information Fig. 6). The
102 portability and combinatorial synergy of these mutations across scaffolds demonstrates the power of
103 this neural network-based approach.

104 Next, we sought to evaluate the PET hydrolytic activity of these more stable variants across a
105 range of temperatures from 30 to 60 °C using an amorphous PET film (gf-PET, from the supplier
106 Goodfellow, PA, USA) commonly used in the literature⁴. This comparison immediately revealed that
107 the machine-learning guided predictions greatly enhanced PET-hydrolytic activity and extended the

108 range of working temperature in all scaffolds (Fig. 1d). In particular, PETase^{N233K/R224Q/S121E} exhibited
109 a 3.4-fold and 29-fold increase in PET-hydrolytic activity at 30 and 40 °C respectively, over wild-type
110 PETase (Fig. 1d). Enzyme mutants based on the ThermoPETase scaffold showed an extended range
111 of working temperature (30–60 °C) and exhibited significantly higher activity than their counterparts.
112 Within this set, the best variant from the ThermoPETase scaffold (containing N233K and R224Q on
113 top of S121E), named FAST-PETase (Functional, Active, Stable, and Tolerant PETase), showed 2.4-
114 fold and 38-fold higher activity at 40 and 50 °C, respectively compared to ThermoPETase alone (Fig.
115 1d). At 50 °C, FAST-PETase displayed the highest overall degradation of all mutants and temperatures
116 activity releasing 33.8 mM of PET monomers in 96 hours (Fig. 1d). The DuraPETase scaffold in
117 general exhibited relatively low activity at mild temperatures (30–50 °C), but improvements were
118 nevertheless realized at higher temperatures (55–60 °C) as demonstrated by the most thermostable
119 PETase mutant- DuraPETase^{N233K} (Fig. 1d).

120 Crystal structure analysis of FAST-PETase at 1.44 Å resolution explains the enhanced stability
121 through newly formed, favorable residue interactions (Fig. 2). The N233K mutation places a
122 positively-charged lysine next to E204 and establishes an intramolecular salt bridge (Fig. 2f). The side
123 chain of R224, when mutated to Gln, forms a hydrogen bond to the carbonyl group of S192 (Fig. 2d).
124 Finally, the S121E mutation enables a new water-mediated hydrogen-bonding network with H186 and
125 N172 (Fig. 2d).

126 To evaluate the catalytic resilience of these mutants to environmental conditions, FAST-
127 PETase were compared to previously reported wild-type and mutant PHEs including wild-type PETase,
128 ThermoPETase, DuraPETase, LCC, the most active mutant LCC^{F243I/D238C/S283C/N246M} (ICCM) using
129 gf-PET across a range of pH (6.5 – 8.0) and temperatures (30–40 °C) (Supplementary Information Fig.
130 7). This comparative analysis demonstrated the unique catalytic capability of FAST-PETase to
131 function at low pH levels and ambient temperature. Specifically, FAST-PETase outperformed other
132 PHEs (including prior rational designs) at all pH conditions. Especially at pH 7, FAST-PETase

133 exhibited activities that were 9.7 and 115 times as high as that of wild-type PETase at 30 and 40 °C,
134 respectively ([Supplementary Information Fig. 7](#)). This enzymatic performance makes FAST-PETase
135 an excellent candidate for mild temperatures and moderate pH enzymatic degradation of PET seen in
136 conditions of *in situ* plastic degradation.

137 Beyond model plastic substrates, it is critical to demonstrate the performance of PETase
138 enzymes on raw, untreated pc-PET. Notably, unlike the gf-PET used above and throughout the
139 literature, there is no singular pcPET substrate. To this end, we collected 51 samples of post-consumer
140 plastic products used in the packaging of food, beverages, medications, office supplies, household
141 goods and cosmetics available at local grocery store chains and treated this raw material enzymatically
142 with FAST-PETase at 50 °C ([Supplementary Information Fig. 8](#)). Despite their heterogeneity including
143 physical properties such as crystallinity, molecular weight, and thickness as well as different
144 compositions including additives and plasticizers, hole-punched samples from this wide array of PET
145 products were all fully degraded by FAST-PETase within one week and in as little as 24 hours ([Fig.](#)
146 [3a](#)). While thickness of the plastic did correlate with degradation time (as thickness and mass are
147 related), neither this metric nor crystallinity or any other measured trait of PET alone determined
148 overall degradation rates ([Supplementary Information Fig. 9](#)).

149 Among the post-consumer products tested above, we further evaluated the sample from a bean
150 cake container that was completely degraded by FAST-PETase within 24 hrs at 50 °C. A time-course
151 analysis ([Fig. 3b](#)) revealed that the degradation of this pc-PET film exhibited an almost linear decay
152 rate using FAST-PETase in terms of the total PET monomers released. Concomitantly, degradation of
153 the pc-PET film by FAST-PETase brought an increase in the crystallinity from 1.2 % to 7.7% over 24
154 hrs ([Supplementary Information Fig. 10](#)). Atomic Force Microscopy ([Fig. 3c](#)) as well as Scanning
155 Electron Microscopy ([Supplementary Information Fig. 11](#)) further showed that the reaction
156 progression of FAST-PETase as it produced increasingly deeper and larger holes in the pc-PET surface
157 resulting in increased surface roughness (and visible opaqueness) over reaction time ([Supplementary](#)

158 Information Fig. 12). In contrast, the PET-hydrolytic activity of wild-type PETase, ThermoPETase,
159 DuraPETase, LCC and ICCM toward this pc-PET was substantially lower (3.2 to 141.6-fold) than that
160 of FAST-PETase under the same conditions (Fig. 3b). Interestingly, even at their previously reported
161 optimal reaction temperature of 72 °C⁴, the activity of LCC and ICCM was still 4.9-fold and 1.5-fold
162 lower than that of FAST-PETase at 50 °C. Further experimental analysis (Supplementary Information
163 Fig. 13) indicated that LCC and ICCM exhibited their highest degradation rate against this pc-PET
164 film at 60 °C. However, even at 60°C, the activity of LCC and ICCM was still lower than that of FAST-
165 PETase at 50 °C. Moreover, we demonstrate that the depolymerization process with FAST-PETase is
166 easily scalable to large, untreated pieces of plastic (in this case, 6.4 g rather than 11 mg) simply by
167 increasing net reaction volumes (Fig. 3d). Given these results, FAST-PETase can serve as a promising
168 biocatalyst for the enzyme-based platform aimed at recycling raw, untreated PET waste, with
169 advantages of lower operating cost and higher degradation efficiency of pc-PET, in contrast to ICCM
170 that requires a higher reaction temperature.

171 Beyond packaging materials, PET is used heavily in the synthetic textile industry. To this end,
172 we evaluated the potential application of FAST-PETase to partially degrade commercial polyester
173 products. Five different commercial polyester products were treated with FAST-PETase at 50 °C,
174 releasing higher amounts of terephthalic acid (TPA) and Mono-(2-hydroxyethyl)terephthalate (MHET)
175 relative to that of the samples treated with other PHEs (Fig. 3e). This indicates that FAST-PETase can
176 potentially be used for rapid and efficient degradation of the PET fragments embedded in textile fabrics,
177 providing a potential route for recovering PET monomers from commercial polyester products and
178 reducing the leaching of microfibers into the environment.

179 Given the high activity of this FAST-PETase mutant at ambient temperatures and pH
180 conditions, we hypothesized that this enzyme would be suitable for various enzymatic-microbial and
181 enzymatic-chemical processing of PET. In this regard, PET depolymerization is only half of the
182 circular plastic economy and we demonstrate here the compatibility of FAST-PETase with both

183 chemical and biological recycling/upcycling applications to close the cycle. First, we demonstrate a
184 closed-cycle PET re-constitution by first depolymerizing a tinted post-consumer plastic waste utilizing
185 FAST-PETase and subsequently recovering monomers. TPA was recovered from the degradation
186 solution with a yield of 96.8% and with a purity of over 99%. We then regenerate virgin PET directly
187 from the degradation solution using chemical polymerization (Fig. 4a). A complete cycle of
188 degradation to re-polymerization can be accomplished in as little as a few days (**Supplementary**
189 **Information Fig. 14**). These results demonstrate the feasibility of a closed-loop enzymatic/chemical
190 recycling process to generate a clear, virgin PET film from non-petroleum resources. Moreover, this
191 workflow bypasses the challenges of recycling mixed-color PET products.

192 Second, we sought to utilize the degradation capability of FAST-PETase at ambient
193 temperature to enable direct depolymerization and microbial valorization of monomers. To this end,
194 we evaluated a simultaneous biodegradation scheme using FAST-PETase to demonstrate that this
195 mutant enzyme is microbe-compatible. In particular, a soil bacteria *Pseudomonas putida* Go19^{20,21}
196 capable of naturally utilizing TPA as a carbon and energy source and capable of producing
197 polyhydroxyalkanoates (PHAs) was employed. Initially, we sought to combine exogenous FAST-
198 PETase with this host to explore the possibility of simultaneous PET depolymerization and
199 fermentation. *P. putida* Go19 was inoculated into a minimal medium supplemented with an
200 unpretreated pc-PET film absent of any other carbon source. Upon adding 200 nM of purified FAST-
201 PETase to the culture medium, growth of *P. putida* Go19 was observed concomitant with the degraded
202 pc-PET film which displayed opacity and lost $20.2 \pm 2.1\%$ of its initial weight (Fig. 4b) after 4 days.
203 Through this experiment, we observed that the TPA liberated from the hydrolysis of pc-PET film by
204 FAST-PETase was consumed by the *P. putida* Go19 for growth (Fig. 4b) and PHAs accumulation (Fig.
205 4c). In contrast, when wild-type PETase, ThermoPETase, DuraPETase, LCC, or ICCM was used as
206 the catalyst in such process, the cell density of *P. putida* Go 19 and the weight loss of the pc-PET film
207 were all significantly lower than when FAST-PETase was used (Fig. 4b). These results demonstrated

208 that FAST-PETase exhibited the highest PET-hydrolytic activity under cell-growth compatible
209 conditions when compared with other PHEs tested. This demonstration represents the first
210 simultaneous bioprocess that integrates enzymatic PET depolymerization and TPA conversion to
211 PHAs at ambient temperatures and neutral pH.

212 In conclusion, this work utilized a structure-based deep learning model to identify portable
213 substitutions that imparted improved stability and function across a variety of PETase scaffolds. The
214 best variant, FAST-PETase, exhibits superior activity over a wide range of temperatures (30–50 °C),
215 and exceptional compatibility with cell-growth conditions. We demonstrate this capacity via the rapid,
216 efficient, and complete degradation of bulk, untreated pc-PET waste and a reduction of PET fragments
217 embedded in textile fabrics. The properties of this variant are ultimately suitable for both low-cost
218 industrial recycling as well as for *in situ* plastic degradation applications, as demonstrated by
219 simultaneous bioprocessing with *P. putida* Go 19. Collectively, these results demonstrate the potential
220 for structure-based deep learning in protein engineering and the opportunities for converting
221 mesophilic enzyme scaffolds into broad-range biocatalysts for a cyclic plastic economy.

222 **References**

- 223 1. Geyer, R., Jambeck, J. R. & Law, K. L. Production, use, and fate of all plastics ever made. *Sci. Adv.* **3**, (2017).
- 224 2. Chen, C. C., Dai, L., Ma, L. & Guo, R. T. Enzymatic degradation of plant biomass and synthetic polymers. *Nature Reviews Chemistry* (2020). doi:10.1038/s41570-020-0163-6
- 225 3. George, N. & Kurian, T. Recent Developments in the Chemical Recycling of Postconsumer Poly(ethylene terephthalate) Waste. *Ind. Eng. Chem. Res.* **53**, 14185–14198 (2014).
- 226 4. Tournier, V. *et al.* An engineered PET depolymerase to break down and recycle plastic bottles. *Nature* (2020). doi:10.1038/s41586-020-2149-4
- 227 5. Simon, N. *et al.* A binding global agreement to address the life cycle of plastics. *Science* (80-.). **373**, 43 LP – 47 (2021).
- 228 6. Kawai, F., Kawabata, T. & Oda, M. Current knowledge on enzymatic PET degradation and its possible application to waste stream management and other fields. *Applied Microbiology and Biotechnology* **103**, (2019).
- 229 7. Taniguchi, I. *et al.* Biodegradation of PET: Current Status and Application Aspects. *ACS Catal.* (2019). doi:10.1021/acscatal.8b05171
- 230 8. Inderthal, H., Tai, S. L. & Harrison, S. T. L. Non-Hydrolyzable Plastics – An Interdisciplinary Look at Plastic Bio-Oxidation. *Trends in Biotechnology* (2021). doi:10.1016/j.tibtech.2020.05.004
- 231 9. Yoshida, S. *et al.* A bacterium that degrades and assimilates poly(ethylene terephthalate). *Science* (80-.). (2016). doi:10.1126/science.aad6359
- 232 10. Chen, C. C. *et al.* General features to enhance enzymatic activity of poly(ethylene terephthalate) hydrolysis. *Nat. Catal.* (2021). doi:10.1038/s41929-021-00616-y
- 233 11. Worm, B., Lotze, H. K., Jubinville, I., Wilcox, C. & Jambeck, J. Plastic as a Persistent Marine Pollutant. *Annual Review of Environment and Resources* (2017). doi:10.1146/annurev-

- 247 environ-102016-060700
- 248 12. Son, H. F. *et al.* Rational Protein Engineering of Thermo-Stable PETase from Ideonella
249 sakaiensis for Highly Efficient PET Degradation. *ACS Catal.* **9**, 3519–3526 (2019).
- 250 13. Austin, H. P. *et al.* Characterization and engineering of a plastic-degrading aromatic
251 polyesterase. *Proc. Natl. Acad. Sci. U. S. A.* **115**, E4350–E4357 (2018).
- 252 14. Joo, S. *et al.* Structural insight into molecular mechanism of poly(ethylene terephthalate)
253 degradation. *Nat. Commun.* **9**, (2018).
- 254 15. Han, X. *et al.* Structural insight into catalytic mechanism of PET hydrolase. *Nat. Commun.*
255 (2017). doi:10.1038/s41467-017-02255-z
- 256 16. Furukawa, M., Kawakami, N., Oda, K. & Miyamoto, K. Acceleration of Enzymatic
257 Degradation of Poly(ethylene terephthalate) by Surface Coating with Anionic Surfactants.
258 *ChemSusChem* (2018). doi:10.1002/cssc.201802096
- 259 17. Cui, Y. *et al.* Computational Redesign of a PETase for Plastic Biodegradation under Ambient
260 Condition by the GRAPE Strategy. *ACS Catal.* (2021). doi:10.1021/acscatal.0c05126
- 261 18. Chen, K., Hu, Y., Dong, X. & Sun, Y. Molecular Insights into the Enhanced Performance of
262 EKylated PETase Toward PET Degradation. *ACS Catal.* **11**, 7358–7370 (2021).
- 263 19. Shroff, R. *et al.* Discovery of novel gain-of-function mutations guided by structure-based deep
264 learning. *ACS Synth. Biol.* (2020). doi:10.1021/acssynbio.0c00345
- 265 20. Narancic, T. *et al.* Genome analysis of the metabolically versatile *Pseudomonas umsongensis*
266 GO16: the genetic basis for PET monomer upcycling into polyhydroxyalkanoates. *Microb.*
267 *Biotechnol.* (2021). doi:10.1111/1751-7915.13712
- 268 21. Kenny, S. T. *et al.* Up-cycling of PET (Polyethylene Terephthalate) to the biodegradable
269 plastic PHA (Polyhydroxyalkanoate). *Environ. Sci. Technol.* (2008). doi:10.1021/es801010e
- 270
- 271

272 **Figure Legends**

273 **Fig. 1 Machine-learning guided predictions improve enzyme performance across PETase**
274 **scaffolds. a.** Wild-type PETase protein structure rendered by the output of Mutcompute. Each amino
275 acid residue was assessed by Mutcompute, resulting in a probability distribution reflecting the
276 chemical congruency of each of the twenty amino acids with the neighboring chemical
277 microenvironments. Residues assigned the low wild-type probability (disfavored) are red and the high
278 wild-type probability (favored) are blue. Interactive visualizations of MutCompute are available at
279 <https://www.mutcompute.com/petase/5xjh> and <https://www.mutcompute.com/petase/6ij6>. **b.** Using
280 MutCompute with both wild-type PETase and ThermoPETase, two libraries of predictions were
281 generated. To down-select mutations, the predictions were ranked by the fold change in the
282 probabilities between the predicted and the wild-type amino acid. Using a stepwise combination
283 strategy, 159 variants were generated by incorporating single or multiple predicted mutations into
284 various PETase scaffolds. After experimental characterization, four predicted mutations (S121E,
285 N233K, R224Q and T140D) resulted in the highest improvements both singly and in combination. **c.**
286 Microenvironment of the four major mutations predicted by Mutcompute. **d.** The four major mutations
287 were completely and combinatorially assembled across three PETase scaffolds: wild-type PETase
288 (WT), ThermoPETase (Thermo), and DuraPETase (Dura). The red heatmap (left) shows the PET-
289 hydrolytic activity of the resulting variants and the blue heatmap (right) shows the fold-change of
290 activity over their respective scaffolds. PET-hydrolytic activity was evaluated by measuring the
291 amount of PET monomers (the sum of TPA and MHET) released from hydrolyzing circular gf-PET
292 film (6 mm in diameter, ~11.4 mg) by the PETase variants after 96 hrs of incubation at temperature
293 ranging from 30 to 60 °C. All measurements were conducted in triplicate (n=3).

294

295 **Fig. 2 Predicted mutations from neural network algorithm stabilizes FAST-PETase. a-f.**
296 Structural comparison between (**a, c, e**) wild-type PETase (tan-colored stick model, PDB code: 5XJH)

297 and **(b, d, f)** FAST-PETase (blue-colored stick model, PDB code: 7SH6) near the predicted mutation
298 sites (S121E, R224Q, N233K respectively). Hydrogen bonding and salt bridge interactions are shown
299 and highlighted as yellow dotted lines.

300

301 **Fig. 3 The superior performance of FAST-PETase in enzymatic depolymerization of post-**
302 **consumer PET plastic and polyester products.** **a.** Complete degradation of pc-PET films hole-
303 punched from 51 post-consumer plastic products. **b.** Time-course of PET-hydrolytic activity of FAST-
304 PETase, wild-type PETase (WT), ThermoPETase (Thermo), DuraPETase (Dura), LCC and ICCM at
305 reaction temperature of 50 °C. PET-hydrolytic activity was evaluated by measuring the amount of PET
306 monomers (the sum of TPA and MHET) released from hydrolyzing pc-PET (Bean cake plastic
307 container) film by the tested PHEs at various time points. KH₂PO₄-NaOH (pH 8) buffer was used for
308 all enzymes shown in this figure. All measurements were conducted in triplicate (n=3). **c.** Atomic
309 Force Microscopy images of pc-PET films following various exposure times with FAST-PETase. **d.**
310 Complete degradation of large, untreated PET container with FAST-PETase at 50 °C. **e.** Degradation
311 of commercial polyester products with FAST-PETase, wild-type PETase (WT), ThermoPETase
312 (Thermo), DuraPETase (Dura), LCC and ICCM at 50 °C. All measurements were conducted in
313 triplicate (n=3).

314

315 **Fig. 4 Applications of FAST-PETase in enzymatic-chemical recycling of PET and *in situ***
316 **depolymerization.** **a.** Schematic of the closed-loop PET recycling process incorporating post-
317 consumer colored plastic waste depolymerization by FAST-PETase and chemical polymerization. The
318 crystallinity of the regenerated PET was determined as 58 % by Differential Scanning Calorimetry.
319 The molecular weights (M_n, M_w), polydispersity indices (D) of the regenerated PET were determined
320 as M_n = 16.4 kg/mol, M_w = 45.9 kg/mol, D = 2.80 by Gel Permeation Chromatography. **b.**

321 Simultaneous process combining *P. putida* Go19 and exogenous PHEs: FAST-PETase, wild-type
322 PETase (WT), ThermoPETase (Thermo), DuraPETase (Dura), LCC and ICCM. PHE (FAST-
323 PETase/WT/Thermo/Dura/LCC/ICCM) & Go19 represents the simultaneous process of a PHE with
324 *P. putida* Go 19, whereas PHE alone represents the control condition where the enzyme is presented
325 without *P. putida* Go 19. PET monomers, mass loss of the pc-PET films, and cell density of *P. putida*
326 Go19 were measured after 96 hrs of incubation. All measurements were conducted in triplicate (n=3).
327 EG represents ethylene glycol. **c.** Bright field (BF) microscopy of *P. putida* Go19 cells after growth
328 with pc-PET film for 96 hrs, and fluorescent microscopic observation of the intracellular PHAs
329 granulate via Nile Red (NR) staining of same cells.

330

331 **Acknowledgements**

332 This work was funded under research agreement EM10480.26 / UTA16-000509 between the
333 ExxonMobil Research and Engineering Company and The University of Texas at Austin. Sequencing
334 was conducted at the Genomic Sequencing and Analysis Facility and Scanning Electron Microscopic
335 analysis was conducted at the Microscopy and Imaging Facility at the UT Austin Center for
336 Biomedical Research Support. We acknowledge Dr. Sapun Parekh (The University of Texas at Austin)
337 for access to his microscopic imaging facility, as well as Yujen Wang for his assistance in taking
338 microscopic fluorescent images.

339

340 **Accession number**

341 Coordinates for the FAST-PETase structure have been deposited into the Protein Data Bank with
342 accession code 7SH6.

343

344

345

346 **Author contributions**

347 H.A., A.E., N.L., and H.L. designed and directed the research. In investigation and validation, R.S.
348 and D.D. performed neural network analysis, H.L. performed enzyme engineering, purification, and
349 the simultaneous process experiment. H.L., N.C., C.Z., D.A. and H.C. carried out structural and
350 physical characterization of variants. C.Z. and N.C. performed physical characterization of the treated
351 and untreated commercial PET materials. C.Z carried out experiments for purifying terephthalic acid
352 and regenerating virgin PET and plastics films. D.D. and B.A. developed MutCompute-View for
353 visualizing predictions from the neural network model W.K. and Y.Z. performed protein
354 crystallization and structural analysis of the engineered enzyme. H.A. and H.L. wrote the original draft
355 of the manuscript H.A., A.E., N.L., and H.L. revised the manuscript. H.A. and A.E. conceived the
356 project idea. All authors reviewed and accepted the manuscript.

357

358 **Competing interests**

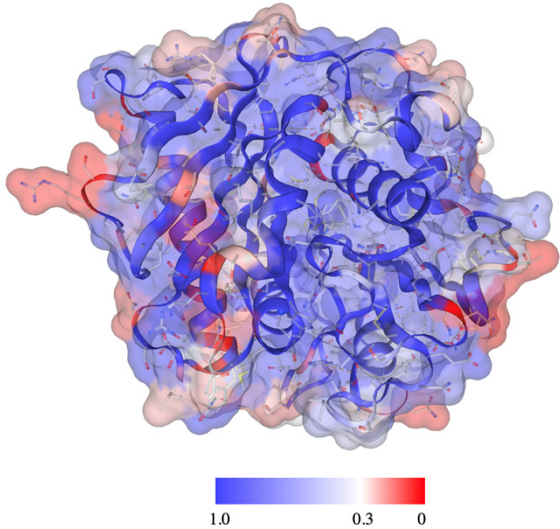
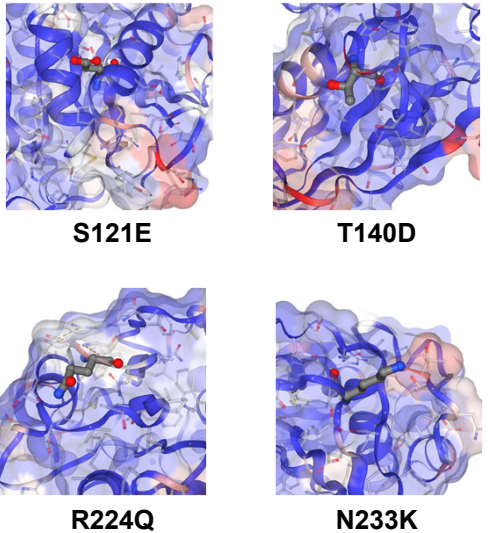
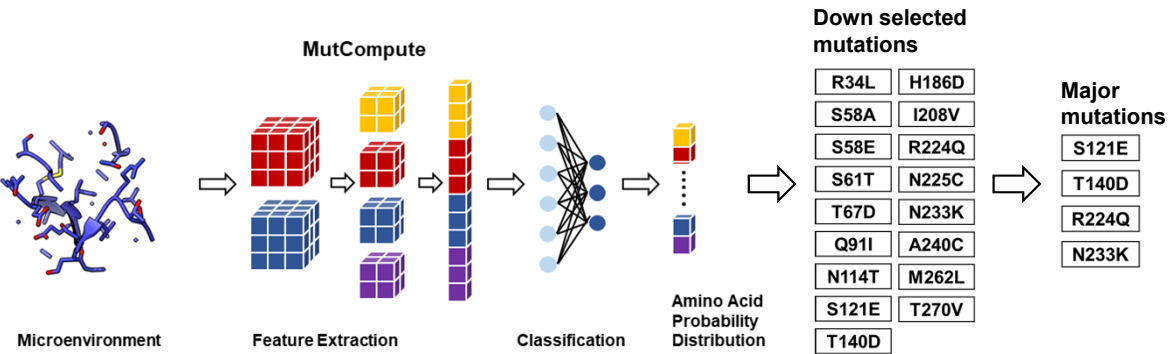
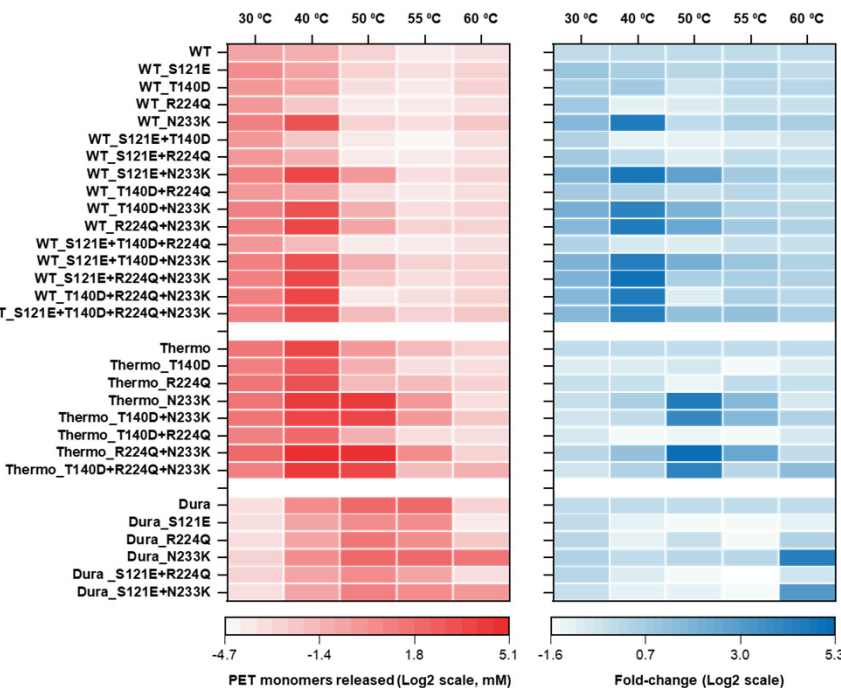
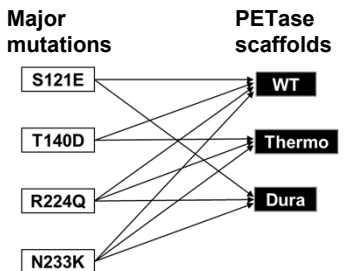
359 A patent has been filed in 2020, “Mutations for improving activity and thermostability of PETase
360 enzymes” relating to the mutants and applications developed in this study. R.S. is a co-founder of
361 Aperiam, a company that applies machine learning to protein engineering. R.S. and A.E. are inventors
362 on a patent for applying machine learning to protein engineering, that has been licensed to Aperiam.

363

364 **Additional Information**

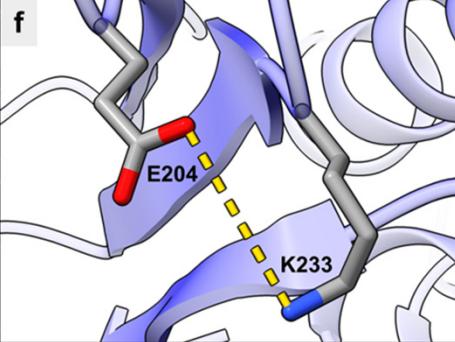
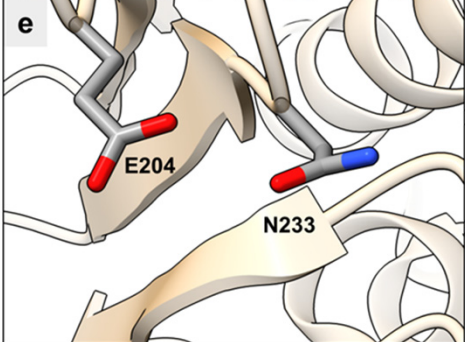
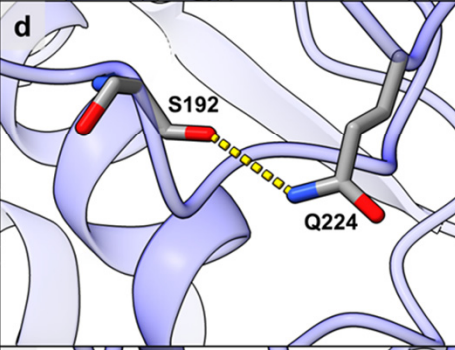
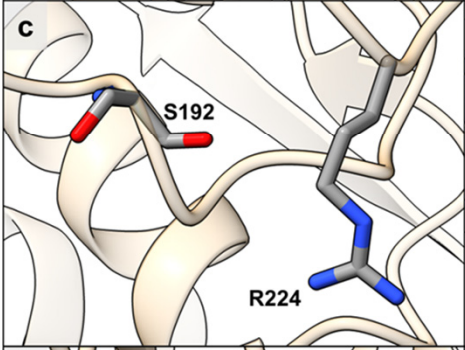
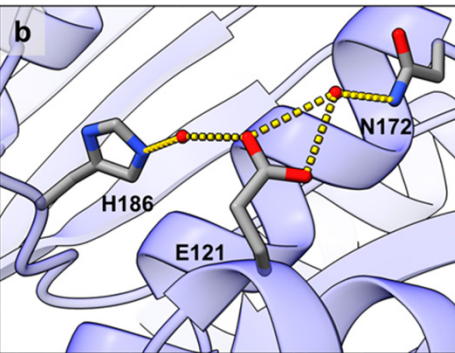
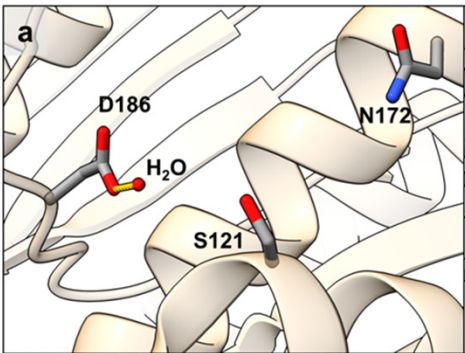
365 **Supplementary Information** is available for this paper.

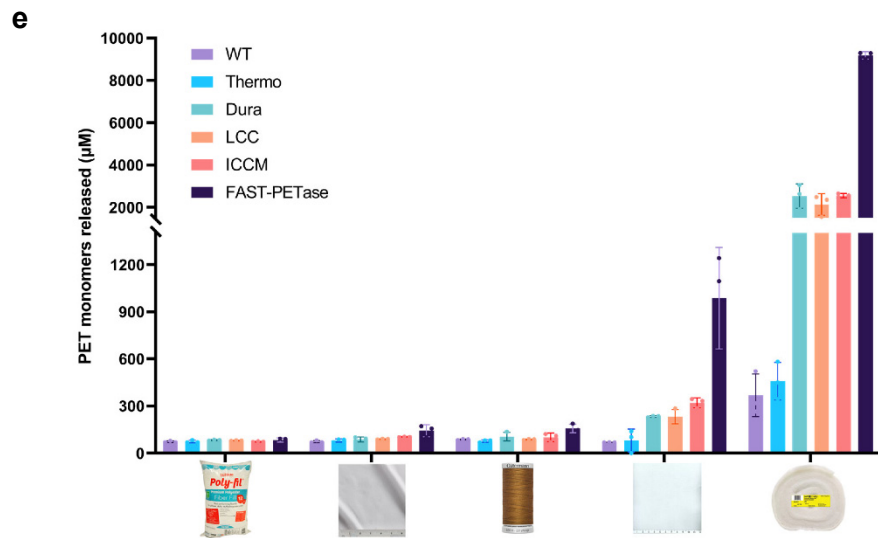
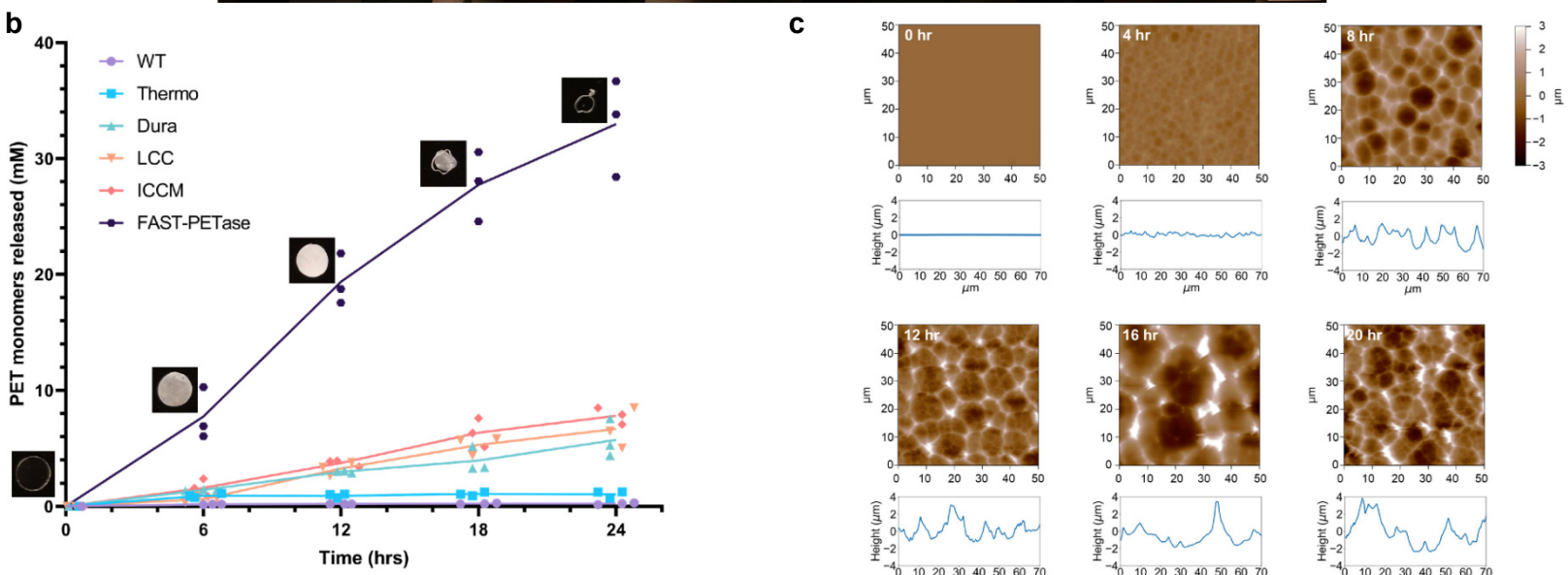
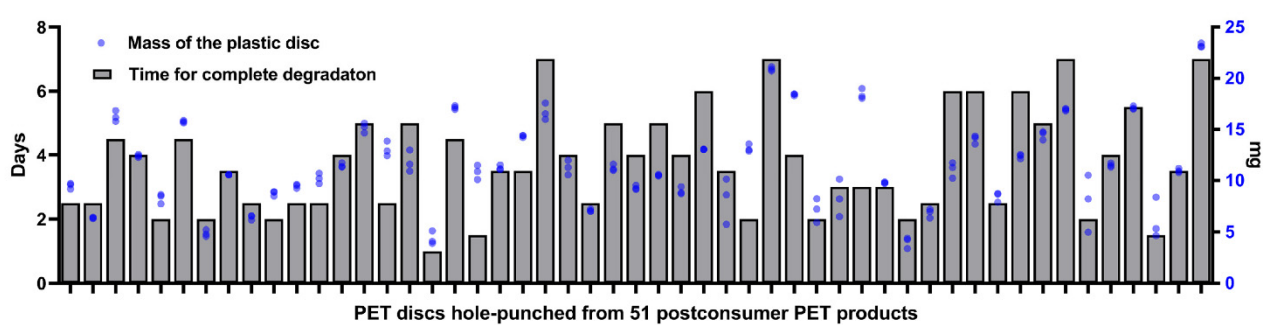
366 **Correspondence and requests for materials** should be addressed to H.A.

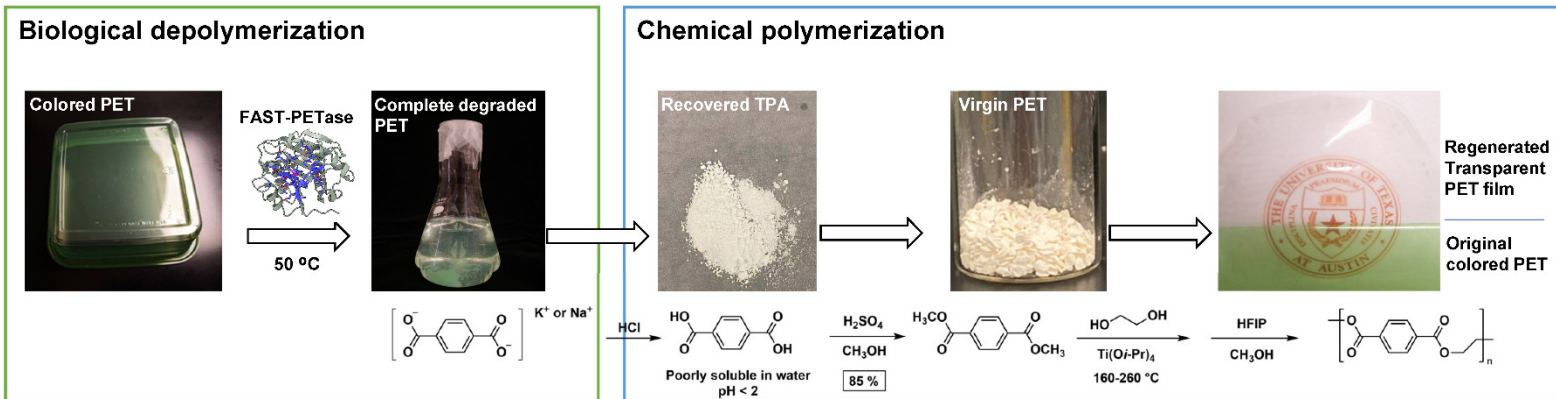
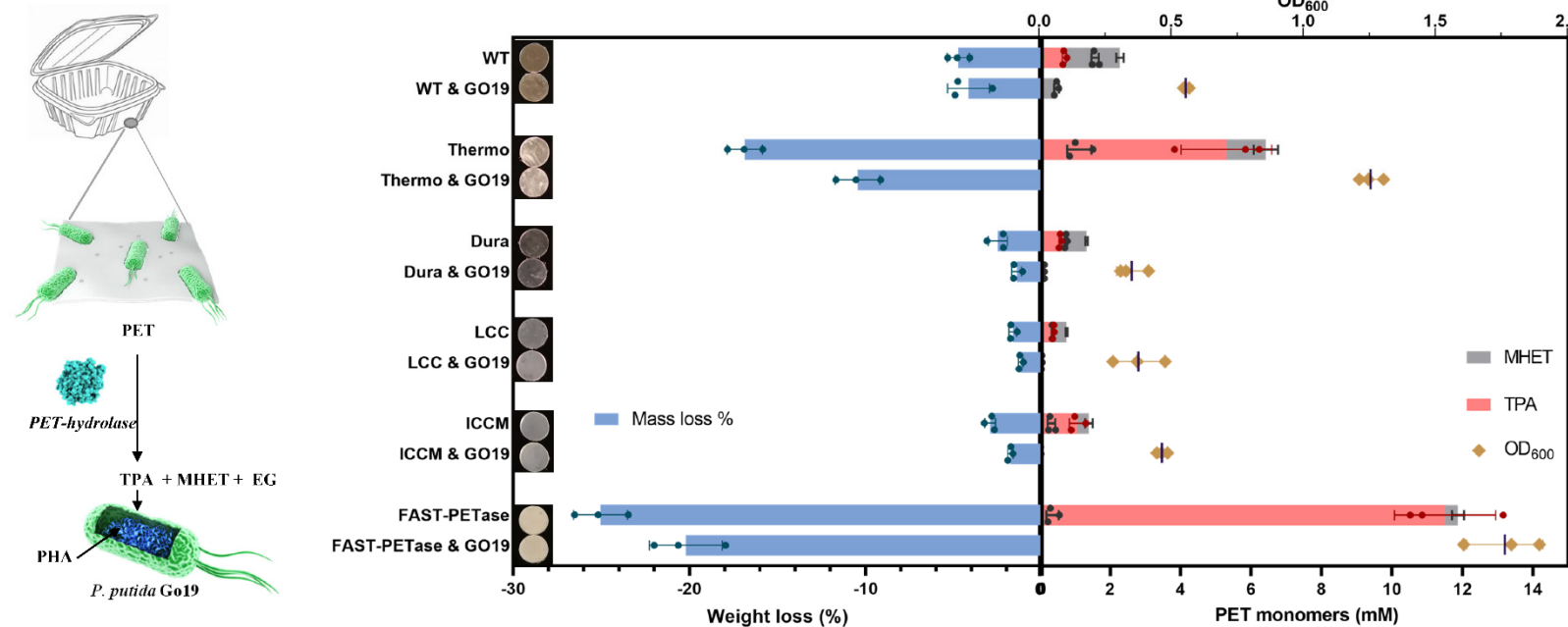
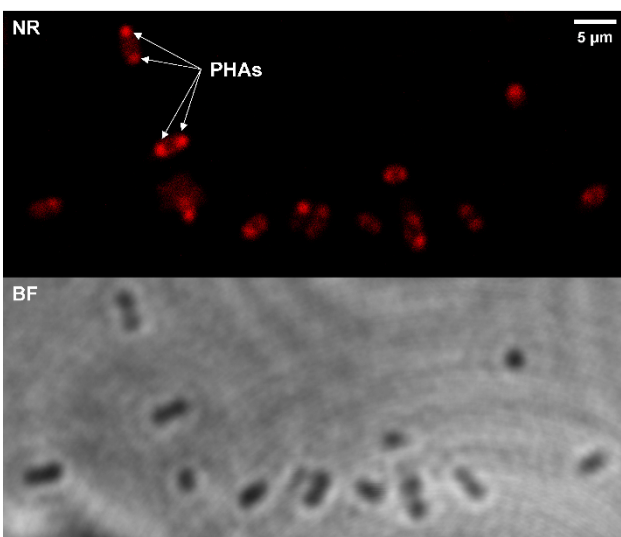
a**c****b****d**

WT - PETase

FAST - PETase





a**b****c**

367 **Supplementary Methods**

368 **Supplementary Methods 1:** Description of methods

369 **Convolutional Neural Network (CNN) Model:**

370 MutCompute¹⁹ is a 3D CNN model where the architecture consists of nine layers divided into two
371 blocks: 1) feature extraction and 2) classification. The feature extraction block consisted of six layers:
372 two pairs of 3D convolutional layers followed by a dimension reduction max pooling layer after each
373 pair. The first pair of convolutional layers used filters of size 3x3x3 and the second pair had filters of
374 size 2x2x2. Additionally, the Rectified Linearity Unit function (Relu) was applied to the output of each
375 of the four convolutional layers. The final feature maps generated by the feature extraction block had
376 dimensions of size 400x3x3x3. These feature maps were flattened into a 1D vector of size 10,800
377 before being passed to the classification block. The classification block consisted of three fully
378 connected dense layers given dropout rates of 0.5, 0.2, and 0, respectively. Like the feature extraction
379 block, the output of the first two dense layers was transformed by the Relu function. To obtain a vector
380 of 20 probability scores representing the network prediction for each of the amino acids, we applied a
381 softmax activation function to the output of the third dense layer. MutCompute is available as a
382 machine learning as a service (MLaaS) on <https://mutcompute.com>.

383 **MutCompute Predictions:**

384 MutCompute predictions were obtained by running the wild type PETase (pdb id: 5xjh) and
385 thermopetase (pdb id: 6ij6) through our MLaaS at <https://mutcompute.com>. Residues were filtered by
386 sorting by the probability assigned to the wild type amino acid. We filtered 34 and 39 residues from
387 the wild type PETase and Thermopetase crystal structures, respectively. From these filtered residues,
388 we prioritized our experimental mutagenesis by selecting the 10 residues from each crystal structure
389 with the highest log2 fold change between the predicted amino acid and wild type amino acid
390 probabilities. Prior to experimentation, selected residues were visualized with Mutcompute-View,

391 which is built on top of NGLViewer (<https://github.com/nglviewer/ngl>), to ensure three things: 1) the
392 prediction was chemically sound and not due to a crystal or model artifact, 2) we were avoiding the
393 active site and binding pocket and 3) avoiding epistatic interactions between predictions and instead
394 targeting predicted “instability hotspots”. MutCompute-View has been made publicly available at
395 <https://mutcompute.com/view>.

396

397 **Protein crystallization, X-ray diffraction data collection, data processing, and model**

398 **refinement**

399 To identify crystallization conditions for FAST-PETase, a sample containing 6 mg/mL purified FAST-
400 PETase was screened in sparse-matrix screening using Phoenix robotic system (Art Robinson). The
401 initial hits were identified with the rod-shaped crystals formed after incubating screening plates at
402 25 °C for three days. The crystallization was optimized as 0.1 M bis-TRIS, 2.0 M Ammonium Sulfate,
403 pH 5.5 setup as sitting-drop vapor diffusion.

404

405 Individual FAST-PETase crystals were flash-frozen directly in liquid nitrogen after cryoprotected with
406 30 % (v/v) glycerol. X-ray diffraction data were collected at 23-ID-B beamline in Advance Photon
407 Source (Lemont, IL). The X-ray diffraction pattern was processed to 1.44 Å resolution for FAST-
408 PETase crystals using HKL2000²². The structure was solved by molecular replacement with
409 ThermoPETase structure as the initial search model (PDB code 6IJ6¹²). The molecular replacement
410 solution for FAST-PETase structure was iteratively built and refined using Coot²³ and Phenix²⁴
411 refinement package. Procheck and MolProbity evaluated the quality of the finalized FAST-PETase
412 structure. The final statistics for data collection and structural determination are shown in
413 **Supplementary Information Fig. 18.**

414

415 **Cloning**

416 Genes encoding *Ideonella sakaiensis* 201-F6 *IsPETase* (wild-type PETase) (Genbank:
417 BBYR01000074, *ISF6_4831*), its mutants—PETase S121E/D186H/R280A (ThermoPETase¹²) and
418 PETase^{S214H/I168R/W159H/S188Q/R280A/A180I/G165A/Q119Y/L117F/T140D} (DuraPETase¹⁷), leaf-branch compost
419 cutinase (LCC) (Genbank: AEV21261) and its mutant LCC F^{243I/D238C/S283C/N246M} (ICCM)⁴ were
420 commercially synthesized for cloning. To enable extracellular expression of PETase and its mutants
421 in *Pseudomonas putida* KT2440 (ATCC 47054), the nucleotide sequence of the signal peptide—
422 SP_{stu} (21 amino acids) from maltotetraose-forming amylase of *Pseudomonas stutzeri* MO-19²⁵ was
423 used to substitute the original signal peptide sequence (first 27 amino acids) of wild-type PETase. The
424 wild-type PETase and its mutants' genes with SP_{stu} presented at the N-terminus were amplified by
425 polymerase chain reaction (PCR) using the synthetic genes as a template. Subsequently, using Gibson
426 Assembly method, DNA fragments encoding wild-type PETase, ThermoPETase and DuraPETase
427 were respectively subcloned into a modified **pBTK552** vector²⁶ where the antibiotic resistance marker
428 was swapped from spectinomycin to kanamycin resistance gene and a C-terminal hexa-histidine tag-
429 coding sequence was added. To enable intracellular expression of LCC and ICCM in *Escherichia coli*
430 (DE3) (New England Biolabs, Ipswich, MA), the nucleotide sequence encoding the original signal
431 peptide was removed from the synthetic genes. The LCC and ICCM genes without signal peptide
432 sequence were amplified by PCR using the synthetic genes as a template. Subsequently, using Gibson
433 Assembly method, the DNA fragments encoding LCC and ICCM were respectively subcloned into a
434 commercial vector-pET-21b (Novagen, San Diego, CA), which carry a C-terminal hexa-histidine tag-
435 coding sequence. The electrocompetent cell *E. coli* DH10 β was transformed with the Gibson Assembly
436 product by following a standard electroporation protocol. The resultant expression plasmid DNA was
437 extracted from the overnight culture of the cloning host by using the QIAprep Spin Miniprep kit
438 (Qiagen, Valencia, CA). The DNA sequence of extracted plasmid was verified by Sanger sequencing.

439 List of nucleotide sequences and expressed amino acid sequences of the genes used in the study is
440 provided in **Supplementary method 2**.

441

442 **Variant construction**

443 Variants of wild-type PETase, ThermoPETase and DuraPETase were generated through site-directed
444 mutagenesis using the PCR method described in the Q5® Site-Directed Mutagenesis Kit E0552S (New
445 England Biolabs, Ipswich, MA). The constructed plasmids carrying wild-type PETase, ThermoPETase
446 and DuraPETase genes were used as the templates for mutagenesis PCR reaction. The corresponding
447 primer sequences and annealing temperature were designed and generated by using the
448 NEBaseChanger™ tool. Stellar™ Competent Cells (Clontech Laboratories, Mountain View, CA)
449 were used as the cloning host and transformed with the ligated plasmids using the heat-shock method
450 provided in the manufacturer's instruction. Plasmid extraction and sequencing for the variants were
451 performed under the same conditions as described for plasmids carrying wild-type PETase,
452 ThermoPETase and DuraPETase genes.

453

454 **Protein expression and purification**

455 For extracellular protein expression of wild-type PETase, ThermoPETase, DuraPETase, and their
456 variants, *P. putida* KT2440 was used as the expression host and its electrocompetent cell was
457 transformed with the corresponding constructed plasmids. For intracellular protein expression of LCC
458 and ICCM, *E. coli* BL21 (DE3) was used as the expression host and its electrocompetent cell was
459 transformed with the corresponding constructed plasmids. A single colony of an *P. putida* KT2440 or
460 *E. coli* BL21 (DE3) strain harboring one of the constructed plasmids was inoculated into 2 mL of Luria
461 Bertani broth (LB) medium with 50 µg/mL kanamycin and grown overnight at 37 °C/225 rpm. The
462 overnight-grown culture (using 150 µl) was scaled up with 1000-fold dilution in a 500-mL triple

463 baffled shake flask and grown to a cell density of 0.8 (optical density [OD₆₀₀]) at 37 °C/225 rpm.
464 Protein expression was induced by adding 0.2 mM of isopropyl β-D-1-thiogalactopyranoside (IPTG)
465 and cells were cultured for 24 hrs at 30 °C/225 rpm. For isolation of the extracellularly expressed
466 PETase enzymes, the induced cell culture was centrifuged at 14,000 g and 4 °C for 20 mins to obtain
467 the supernatant that accommodates secretory protein. For isolation of the intracellularly expressed
468 LCC and ICCM, the induced cell culture was harvested by centrifugation at 4,000 g and 4 °C for 20
469 mins. Cell pellets were then resuspended in 25 mL of Dulbecco's Phosphate Buffered Saline (DPBS)
470 (Thermo Fisher Scientific, Waltham, MA) pH 7.0 buffer containing 10 mM imidazole, 1 g/L of
471 lysozyme and 5 µl of Pierce™ Universal Nuclease (Thermo Fisher Scientific, Waltham, MA),
472 followed by mixing on a rocker for 20 mins at 4 °C. Subsequently, cells were lysed by sonication and
473 the resulting cell lysate was centrifuged at 14,000 g and 4 °C for 20 mins to obtain the supernatant that
474 contains soluble proteins. Target proteins from the above two type of supernatants were both purified
475 by HisPur™ Ni-NTA Resin (Thermo Fisher Scientific, Waltham, MA) according to the
476 manufacturer's instruction. Desalting of the protein eluent was carried out by using Sephadex G-25
477 PD-10 columns (GE Healthcare, Piscataway, NJ) according to the manufacturer's instruction. All
478 purification and desalting steps were performed at 4° C in a cold room. Afterwards, the purified protein
479 was concentrated to a final volume of 1 mL by the 50 mL, 10KDa cut-off Amicon® Ultra Centrifugal
480 Filters device (EMD Millipore Corporation, Billerica, MA) and preserved in DPBS (pH 7.0). The
481 protein concentration was then determined by using the Coomassie Plus Bradford Assay kit (Thermo
482 Fisher Scientific) and the Infinite M200 PRO microplate reader (Tecan, Männedorf, Switzerland) to
483 measure the absorbance of assay mixtures. The presence and purity of the purified proteins were
484 assessed by sodium dodecyl sulfate-polyacrylamide gel electrophoresis.
485

486 **In Vitro Analysis of PET hydrolytic activity using commercial Goodfellow PET film (gf-PET)**

487 To evaluate the PET hydrolytic activity of PETase and its variants, the homogenous amorphous gf-
488 PET film (Goodfellow, U.S. 577-529-50; specification: 1.3-1.4 g cm⁻³ density, 1.58-1.64 refractive
489 index, 100x10⁻¹³ cm³. cm cm⁻² s⁻¹ Pa⁻¹ permeability to water @25°C, 20-80 x10⁻⁶ K⁻¹ coefficient of
490 thermal expansion, 0.13-0.15 W m⁻¹ K⁻¹ @23°C thermal conductivity) was used as the substrate for
491 degradation assays with the purified PETase enzyme and its variants. The gf-PET film was prepared
492 in a circular form (6 mm in diameter, ~11.4 mg) and was washed three times with 1 % SDS, 20 %
493 ethanol, and deionized water before usage. Subsequently, the gf-PET film was put into a glass test
494 tube and fully submerged in 600 µl of 100 mM KH₂PO₄-NaOH buffer (pH 8.0) with 200 nM purified
495 enzyme. The test tube was tightly capped and wrapped with parafilm to minimize volatilization. The
496 reaction mixture was then incubated at 30/40/50/55/60 °C for 96 hrs. Followed by removing the
497 enzyme-treated gf-PET film from the reaction mixture, the enzyme reaction was terminated by heating
498 at 85 °C for 20 mins. The reaction mixture samples were then centrifuged at 10,000 × g for 5 mins.
499 The supernatant of each sample was further analyzed by High-performance liquid chromatography
500 (HPLC) for quantifying PET monomers released from the PET depolymerization.

501 To compare the PET hydrolytic activity of FAST-PETase with wild-type PETase, ThermoPETase,
502 DuraPETase, LCC, and ICCM across a range of pH (6.5 – 8.0) at 30 °C and 40 °C, similar experimental
503 setup was used. The circular gf-PET film (6 mm diameter, ~11.4 mg) was used as the substrate. The
504 enzyme reactions were performed with 200 nM purified enzyme in 600 µl of 100 mM KH₂PO₄-NaOH
505 buffer with various pH (6.5, 7.0, 7.5 or 8.0) at 30 °C and 40 °C. After incubating the enzyme reaction
506 for 96 hrs, the supernatant of the reaction mixture was also analyzed by HPLC for quantifying PET
507 monomers released from the PET depolymerization.

508

509 **Degradation of post-consumer PET (pc-PET) plastics**

510 Hole-punched pc-PET films (6 mm in diameter) from 51 post-consumer plastic products were serially
511 treated by 200 nM FAST-PETase in 600 μ l of 100 mM KH₂PO₄-NaOH buffer (pH 8.0) at 50 °C. Fresh
512 enzyme solution was replenished every 24 hrs to maximize enzymatic degradation rate for degrading
513 the 51 samples of various pc-PET films.

514 The time-course analysis of degrading a pc-PET film (Bean cake container) by various PET-
515 hydrolyzing enzymes (PHEs) was conducted at 50 °C. The reactions were performed with 200 nM
516 enzyme in 600 μ l of 100 mM KH₂PO₄-NaOH buffer (pH 8.0) and terminated at 6 hrs, 12 hrs, 18 hrs
517 or 24 hrs for quantifying total PET monomers released at each time point.

518 A large, untreated, and transparent pc-PET (Bean cake container, 6.4 g) was treated by 200 nM of
519 FAST-PETase in 100 mM of KH₂PO₄-NaOH buffer (pH 8.0) at 50 °C. The whole piece of transparent
520 PET container was fully submerged in 2.5 L of enzyme solution and completely degraded after 48 hrs.

521

522 **Degradation of polyester product**

523 Five different commercial polyester products were cut into small pieces and used as the substrates that
524 were fully submerged in 600 μ l of 100 mM KH₂PO₄-NaOH buffer (pH 8.0) with 200 nM purified
525 enzyme. Enzyme treatment on these five polyester products was conducted at 50 °C. After 24 hrs of
526 incubation, the reaction was terminated. The enzyme degradation solution was used to determine how
527 much PET monomers were released from hydrolyzing these polyester products by various PHEs.

528 **Degradation of large, untreated pc-PET container and regeneration of virgin PET**

529 A large, untreated, and green colored pc-PET container was cut into small rectangular flakes (*ca.* 1cm
530 \times 3 cm). 3.0 g of the colored pc-PET flakes was serially treated by 200 nM FAST-PETase in 100 mM

531 KH₂PO₄-NaOH buffer (pH 8.0) at 50 °C. 200 nM of fresh enzyme was added to the degradation
532 solution every 24 hrs to maximize enzymatic degradation rate. All the colored pc-PET fragments were
533 completely degraded after 6 days.

534 Upon completion of degradation, the enzyme degradation solution was filtered, and the filtrate was
535 collected for regeneration. The pH of the filtrate was adjusted to pH 11 with NaOH to hydrolyze
536 remaining MHET. The solution was stirred at room temperature for 4 hrs to complete the hydrolysis.
537 The pH of the solution was subsequently adjusted to 2 with 37% HCl. The precipitate was filtered and
538 washed several times with deionized water and dried under vacuum overnight. 4.3 g of TPA was
539 collected and used in the next step without further purification. ¹H NMR (400 MHz, *d*₆-DMSO): 8.03
540 ppm (s, 4H).

541 To a suspension of TPA (4.31 g, 25.9 mmol) in CH₃OH (150 mL), 95% H₂SO₄ (2.0 mL) was added
542 dropwise at room temperature. The mixture was stirred at reflux for 24 hrs and became a clear solution.
543 The reaction mixture was then cooled to room temperature. DMT was subsequently recrystallized from
544 the reaction mixture and collected after filtration. These white crystals were washed with cold CH₃OH
545 and dried under vacuum for 4 hrs to afford DMT (4.12 g) with a yield of 82%. ¹H NMR (400 MHz,
546 CDCl₃): 8.08 ppm (s, 4H), 3.93 ppm (s, 6H).

547 To a three-necked round bottom flask equipped with an air condenser, DMT (4.12 g, 21.1 mmol) was
548 added. The flask was evacuated under vacuum and refilled with nitrogen gas for three times. Ethylene
549 glycol (1.20 mL, 21.5 mmol) was added, followed by the addition of titanium isopropoxide (0.06 mL,
550 0.21 mmol). The mixture was stirred at 160 °C for 1 hour, 200 °C for 1 hour, and 210 °C for 2 hrs
551 under nitrogen. The reaction temperature was further increased to 260 °C, and high vacuum was
552 applied to remove unreacted monomers. The mixture was stirred at 260 °C for 2 hrs and then cooled
553 to room temperature. The resulting PET was dissolved in 1,1,1,3,3-hexafluoro-2-propanol (10 mL)

554 and added dropwise to CH₃OH to remove the catalyst. PET (2.83 g) was collected as white solids after
555 centrifuging and dried under vacuum.

556 **Simultaneous bioprocess combining *P. putida* Go19 and exogenous PHEs**

557 The simultaneous process experiments were performed using nitrogen-limiting M9 medium (NL-M9)
558 containing M9 Minimal Salts (Sigma-Aldrich, St Louis, MO), 1 g/L NaNH₄HPO₄·4H₂O, 0.34 g/L
559 thiamine hydrochloride, 2 mM MgSO₄, and 0.1 mM CaCl₂. *P. putida* Go19 (accession number NCIMB
560 41537) was purchased from National Collection of Industrial, Food and Marine Bacteria (NCIMB
561 Aberdeen, Scotland, UK). A single colony of *P. putida* Go19 was inoculated into 20 mL of LB medium
562 and grown overnight at 30 °C/225 rpm. The overnight-grown culture was centrifuged at 4000 g for 5
563 mins. Cell pellets were then resuspended in 20 mL of NL-M9 medium without any carbon source. The
564 resuspended cells used as inoculum for simultaneous process condition where *P. putida* Go19 and
565 exogenous PHEs were combined to explore the possibility of simultaneous PET depolymerization and
566 fermentation. Subsequently, *P. putida* Go19 was inoculated into 1 mL of NL-M9 medium (to an OD₆₀₀
567 of 0.2) supplemented with an unpretreated circular pc-PET film (hole-punched from a cookies plastic
568 container; 6 mm in diameter and weigh around 6 mg) absent of any other carbon source in a culture
569 tube. 200 nM of exogenous enzyme (FAST-PETase, wild-type PETase, ThermoPETase, DuraPETase,
570 LCC or ICCM) was added to the 1 mL NL-M9 medium inoculated with *P. putida* Go19 as the
571 simultaneous process condition. 200 nM of enzymes were also respectively added to the 1 mL of NL-
572 M9 medium absent of *P. putida* Go19 as the control condition. All conditions were incubated at 37 °C
573 and 165 RPM for 72 hrs, followed by incubation at 30 °C and 225 RPM for another 24 hrs to maximize
574 PHAs production in *P. putida* Go19. The experiments were all performed in biological triplicates. PET
575 monomers concentration of the NL-M9 medium with or without *P. putida* Go19, mass loss of the pc-
576 PET films, PHAs accumulation and cell density of *P. putida* Go19 were determined after 96 hrs of
577 incubation.

578

579 **Analytical method for measuring PET monomers released**

580 HPLC was used to analyze the PET monomers— terephthalic acid (TPA) and Mono-(2-
581 hydroxyethyl)terephthalic (MHET) released from PET depolymerization. The assay samples were
582 filtered with 0.2-μm nylon syringe filters (Wheaton Science, Millville, NJ) prior to running HPLC.
583 Measurement of TPA and MHET was performed using a Dionex UltiMate 3000 (Thermo Fisher
584 Scientific, Waltham, MA) equipped with an Agilent Eclipse Plus C18 column (3.0 × 150 mm, 3.5 μm)
585 with detection wavelength at 260 nm. Column oven was held at 30 °C with 1% acetic acid in water or
586 1% acetic acid in acetonitrile as mobile phase over the course of the 30-min sequence under the
587 following conditions: 1% to 5% organic (vol/vol) for 5 min, 5% to 100% organic (vol/vol) for 8 min,
588 100% organic (vol/vol) for 10 min, 100% to 5% organic for 2 min followed by 5% organic for 5 min.
589 The flow rate was fixed at 0.8 mL min⁻¹. A standard curve was prepared using commercial TPA
590 with ≥98.0% purity or MHET ≥ 98.0% purity (Sigma-Aldrich, St Louis, MO).

591

592 **Analytical method for measuring melting temperature (T_m). of proteins**

593 To evaluate the thermostability of wild-type PETase and its variants, Differential Scanning
594 Calorimetry (DSC) was used to determine their respective T_m . Purified protein samples were
595 concentrated to 300~500 μM using Microcon® Centrifugal Filter 10K Devices (Millipore, Billerica,
596 MA). 10 μL of concentrated protein solution (DPBS buffer pH 7.0) was placed in an aluminum Tzero
597 pan and sealed with a Tzero hermetic lid (TA Instruments, DE New Castle, DE). T_m of the protein
598 samples was analyzed by a DSC250 (TA Instruments, New Castle, DE) with a RCS90 electric chiller.
599 Two DSC procedures were used depending on the anticipated denaturation temperature of the protein.
600 The first DSC method heated from 40 °C to 90 °C at 10 °C/min, held at 90 °C for two minutes, then

601 cooled from 90 °C to 40 °C at –10 °C/min. The second method heated from 20 °C to 70 °C at 10
602 °C/min, held at 70 °C for two minutes, cooled from 70 °C to 40 °C at –10 °C/min. The denaturation
603 temperature of the proteins was measured on the heating ramp trace as the midpoint value at half-
604 height.

605 **Analytical method for determining PET film crystallinity**

606 DSC was used to determine percent crystallinity of the PET films hole-punched from the post-
607 consumer plastics. PET film samples (4–10.5 mg) were placed in aluminum Tzero pans with a Tzero
608 solid sample lid. Samples were run first heated from 40 °C to 300 °C at 5 °C/min, held at 300 °C for
609 one minute, cooled from 300 °C to 30 °C at –5 °C/min, held at 30 °C for one minute in a DSC250 (TA
610 Instruments, New Castle, DE) with a RCS90 electric chiller. The percent crystallinity was determined
611 on the first heating scan using the enthalpies of melting and cold crystallization. The equation used to
612 calculate percent crystallinity within the PET film was the following

613
$$\% \text{ crystallinity} = \left[\frac{\Delta H_m - \Delta H_{cc}}{\Delta H_m^\circ} \right] \times 100$$

614 where ΔH_m is the enthalpy of melting (J/g), ΔH_{cc} is the enthalpy of cold crystallization (J/g), and ΔH_m°
615 is the enthalpy of melting for a 100% crystalline PET sample, which is 140.1 J/g^{4,27}. ΔH_m and ΔH_{cc}
616 were measured by integrating from 90–100 °C to *ca.* 260 °C with a linear baseline. The percent
617 crystallinity was calculated using the TRIOS software package. The glass transition temperatures of
618 the PET films were measured using the second heating scan: 30–300 °C at 10 °C/min, held at 300 °C
619 for one minute, then 300–40 °C at –10 °C/min. The glass transition temperatures for all the PET films
620 were between 80–82 °C.

621 **Gel Permeation Chromatography (GPC)**

622 GPC measurement was performed at an on an Agilent system with a 1260 Infinity isocratic pump,
623 degasser, and thermostated column chamber held at 30 °C. A mixture of chloroform with 50 ppm
624 amylene and 1,1,1,3,3-hexafluoro-2-propanol (2.0 vol%) was used as the mobile phase at 0.5
625 mL/min. Molecular weights (M_n, M_w) and polydispersity indices (D) were determined relative to
626 polystyrene standards.

627 Sample preparation for GPC:

628 About 8 mg of PET was dissolved in 0.15 mL 1,1,1,3,3-hexafluoro-2-propanol. Once PET was
629 completely dissolved, chloroform was added to make a total volume of 2.50 mL. The solution was
630 filtered through a PTFE membrane with a pore size of 0.45 µm. 100 µL of the sample solution was
631 then injected into the GPC system.

632 **Scanning Electron Microscopy (SEM)**

633 PET films were mounted onto a 3.2 mm SEM stub using carbon tape. Samples were sputter-coated
634 with 8 nm platinum/palladium using a Cressington 208HR Sputter Coater. The metal was sputter
635 coated onto the sample *via* plasma generated with argon present in the chamber. SEM imaging was
636 performed under vacuum using a Zeiss Supra40 Scanning Electron Microscope (SEM). The electron
637 beam intensity was 5 kV.

638 **Atomic force Microscopy (AFM)**

639 AFM was performed on an Aylum MFP-3D atomic force microscope (Asylum Research, Santa
640 Barbara, CA) in tapping mode. Images were recorded after a surface scan on an area of 50×50 µm.
641 Image analysis including histogram, and surface roughness was performed using Igor Pro.

642

643 **Nuclear magnetic resonance (NMR) spectroscopy**

644 ¹H NMR spectroscopy was performed at a 400 MHz Bruker AVANCE NEO spectrometer at room
645 temperature in CDCl₃ or d₆-DMSO. Chemical shift was referenced to the residual solvent signal (¹H
646 NMR: 7.26 ppm in CDCl₃, 2.50 ppm in d₆-DMSO, respectively).

647 **Microscopic observation of *P. putida* Go19 and PHAs**

648 PHAs formation in *P. putida* Go19 from the simultaneous experiment was microscopically observed
649 by using an upright laser scanning confocal microscope (LSM-510, Zeiss) under reflectance using a
650 100X, 1.3 NA oil-dipping objective (Zeiss), according to the protocol described by Franden et al.²⁸.
651 0.5 mL sample was taken from the simultaneous process experiment of the *P. putida* Go19 culture
652 (with 200 nM of FAST-PETase) that grew on NL-M9 medium supplemented with a circular pc-PET
653 film (cookie container) as the sole carbon source. Culture was centrifuged at 4,000 g for 3 min,
654 followed by washing twice with DPBS. Cell pellets were then stained with 1 mL of 10 µg/mL Nile
655 Red (Thermo Fisher Scientific, Waltham, MA, USA) and kept in the dark for 30 min at room
656 temperature. Subsequently, the stained cells were pelleted again by centrifugation at 4,000 g for 3 min,
657 followed by washing twice with DPBS. Finally, the stained cells were resuspended in 200 µL of DPBS.
658 1 ul of the stained cell solution was dipped on a coverslip and pressed with a small coverslip. The
659 samples were illuminated with a 561 nm laser and reflected light was collected by setting the Meta
660 detector channel between 570-670 nm wavelength.

661 **Additional references**

662

663 22. Otwinowski, Z. & Minor, W. Processing of X-ray diffraction data collected in oscillation
664 mode. *Methods Enzymol.* **276**, 307–326 (1997).

665 23. Emsley, P. & Cowtan, K. Coot: model-building tools for molecular graphics. *Acta*

- 666 *Crystallogr. D. Biol. Crystallogr.* **60**, 2126–2132 (2004).
- 667 24. Liebschner, D. *et al.* Macromolecular structure determination using X-rays, neutrons and
668 electrons: recent developments in Phenix. *Acta Crystallogr. Sect. D, Struct. Biol.* **75**, 861–877
669 (2019).
- 670 25. Fujita, M. *et al.* Cloning and nucleotide sequence of the gene (amyP) for maltotetraose-
671 forming amylase from Pseudomonas stutzeri MO-19. *J. Bacteriol.* (1989).
672 doi:10.1128/jb.171.3.1333-1339.1989
- 673 26. Leonard, S. P. *et al.* Genetic Engineering of Bee Gut Microbiome Bacteria with a Toolkit for
674 Modular Assembly of Broad-Host-Range Plasmids. *ACS Synth. Biol.* (2018).
675 doi:10.1021/acssynbio.7b00399
- 676 27. Cui, Y.-L. *et al.* Computational redesign of PETase for plastic biodegradation by GRAPE
677 strategy. (2019). doi:10.1101/787069
- 678 28. Franden, M. A. *et al.* Engineering Pseudomonas putida KT2440 for efficient ethylene glycol
679 utilization. *Metab. Eng.* **48**, 197–207 (2018).
- 680

681 **Supplementary method 2:**

682 Sequences used in this study

Nucleotide sequence of the signal peptide—SP_{psstu} (21 amino acids) from maltotetraose-forming amylase of *Pseudomonas stutzeri* MO-19²⁵

atgagccacatcctgcgagccgcgtattggcgccatgttgtccgttgcgcgtccatggcc

683

684 **Wild-type PETase**

Nucleotide sequence of wild-type PETase without its original signal peptide

cagaccaatccgtatgcgcgcggccgaatccgacagccgcaggttgaagcgagcgctggccattcaccgtcgctccattaccgtgagt
agaccgagcggttatggcgctggcaccgttactatccaacaatgctgggggtaccgtggcgccatagccatagttcccggtatacggc
acggcagtcatcaattaaatgggggaccgcgtctggcatcccacggttcgttagtaattacaatttgacacaattccacgttagaccagccat
caagtcggagttcgcacaacaatggccgcgtgcgcagggtggcgtttaacggtaactgtagcagccgattacggaaagggtcgatac
cgctcgatgggttatgggtggagttatgggaggtggaggctccctgatctctgctgctaacaacccttcgtgctgaaagcagcggcgcctca
agcaccatggattctcgacaaattttactgttaactgtgccacgctgatctcgcatgtgaaaacgatagttatagccccggtaactctca
gcacttcatatctatgattctatgtcacgcacgctaaggcgtttctgaaattaatggggctcacattctgtgcgaatagcggcaattctaacc
aagcattaatcgaaaaaaaaggcggtgcatggatgaaacgtttatggacaatgatacttaggtattctactttgcctgcgagaacccgaatagc
accagagtgtctgatttcgtacagcgaattgcagcctcgagcaccaccaccaccac

685

Expressed amino acid sequence of wild-type PETase by *P. putida* GO16/KT2440

QTNPYARGPNPTAASLEASAGPFTVRSFTVSRPSGYGAGTVYYPTNAGGTVGAIIVPGY
TARQSSIKWWGPRLASHGFVVITIDNSTLDQPSSRSSQQMAALRQVASLNGTSSSPIYGK
VDTARMGVGMWSMGGGSLISAANNPSLKAAAPQAPWDSSTNFSSVTVP TLIFACENDSI

APVNSSALPIYDSMSRNAKQFLEINGGSHSCANGNSNQALIGKKVAVMKRFMDNDTR
YSTFACENPNSTRVSDFRTANCSLEHHHHH

686

687 **ThermoPETase**

Nucleotide sequence of ThermoPETase without its original signal peptide sequence

cagaccaatccgtatgcgcgcggccgaatccgacagccgccagtttgaagcgagcgctggcattaccgtcgctccattaccgtgagt
agaccgagcggttatggcgctggcaccgttactatccaacaatgctggggtagccgtggcgccatagccatagttcccggtatacggc
acggcagtcatcaattaaatgggggaccgcgtctggcatcccacggttcgttagtaattacaattgacacaaattccacgttagaccagcca
gaaagtccggagttcgcaacaatggccgcgtcgccagggtggcgctgttaaacggtacaagttagcagccgattacggaaagggtcgata
ccgctcgatgggttatgggtggagttatggggtagatggggagggtggaggctccctgatctctgtctgtaacaacccttcgtgaaagcagcggcgccctc
aagcaccatggcactttcgacaaatttttagttctgttaactgtgccacgctgatcttcgcattgtgaaaacgatagtatagccccggtaacttttc
agcacttcctatctatgattctatgtcacgcaacgctaaggcagttctcgaaattaatggtggtcacattcctgtgcgaatagcggcaattctaacc
caaggcattaaatcgaaaaaaaaggcggtgcattggatgaaacggtttatggacaatgatacttaggtattctactttgcctgcgagaacccgaatag
caccgcagtgtctgatttcgtacagcgaattgcagcctcgagcaccaccaccaccac

688

Expressed amino acid sequence of ThermoPETase by *P. putida* KT2440

QTNPYARGPNPTAASLEASAGPFTVRSFTVSRPSGYGAGTVYYPTNAGGTVGAIIVPGY
TARQSSIKWWGPRLASHGFVVITIDTNSTLDQPESRSSQQMAALRQVASLNGTSSSPIYGK
VDTARMGVGMWSMGGGSLISAANNPSLKAAAPQAPWHSSTNFSSVTVP TLIFACENDSI
APVNSSALPIYDSMSRNAKQFLEINGGSHSCANGNSNQALIGKKVAVMKRFMDNDTR
YSTFACENPNSTA VSDFRTANCSLEHHHHH

689

690 **DuraPETase**

Nucleotide sequence of DuraPETase without its original signal peptide sequence

cagaccaatccgtatgcgcggcgtccgaatccgacagccgccagtttggaaagcgagcgctggcattcaccgttcgtccattaccgtgactatccatc
agaccgagcggttatggcgctggcaccgttactatccaacaaatgctggggtaccgtggcgccatgccatagtcccggtatacgcc
acggcagtcatcaattaaatgggggaccgcgtctggcatcccacggttcgttagtaattacaattgacacaaaattccacgttgactatccatc
aagtccggagttcgcacaacaaatggccgcgtgcgcagggtggcgttaaacggtgacagtagcagccccgattacggaaaggcgatacc
gctcgatgggttatgggcatagtatgggagggtggagcatccctgcgatctgctgctaacaaccctcgctgaaagcagcgattcctcaag
caccatgggattctcaaacaattttagttctgtaactgtgcccacgctgatctcgcattgtgaaaacgatagtatagccccgtcaactctcatgc
acttcctatctatgattctatgtcacgcaacgctaaggcagttctcgaaattaatggtgctcacattcctgtgcgaatagcggcaattctaaccaa
gcattaatcgaaaaaaaaggcggtgcatggatgaaacgtttatggacaatgataacttaggtattctactttgcctgcgagaacccgaatagcac
cgcagtgtctgatttcgtacagcgaattgcagcctcgagcaccaccaccaccac

691

Expressed amino acid sequence of DuraPETase by *P. putida* KT2440

QTNPYARGPNPTAASLEASAGPFTVRSFTVSRPSGYGAGTVYYPTNAGGTVGAIIVPGY
TARQSSIKWWGPRLASHGFVVITIDTNSTFDYPSSRSSQQMAALRQVASLNGDSSSPIYGK
VDTARMGVGMHSMGGASLRSAANNPSLKAAIPQAPWDSQTNFSSVTVPTLIFACENDSI
APVNSHALPIYDSMSRNAKQFLEINGSHSCANSQNSNQALIGKKGVAWMKRFMDNDTR
YSTFACENPNSTAVENTSDFRTANCSLEHHHHHH

692

693

694 LCC

Nucleotide sequence of LCC without its original signal peptide sequence

agcaaccgtaccagcgtggccgaatccgacccgcagcgactgaccgagatggcccgttagcgtggcaacctacaccgtctcacgc
ctgtcagtctcggtttggcggtggcgtgatttattaccgcaccggcacgtctgacgttcggcatcgcatgactccggttataccgc
agatgttagtctctggcatggctggcgtcgccctggcttccatggcttgcgtgatataacacgaaattcagttcgattatccggac
agccgcgcctctcagctgagtgccgcctgaactacctgcgtaccagttcccgagcgccgtcgacgtctggatgcaaatcgctggc
ggtgtccggcgtcatttatgggtggcggtggcaccctgcgtattgcagaacaaaacccgagcctgaaagcggctgtcccgtgacccgtggc
acaccgataaaacgttaataccagtgtcccggtctgattgtggcgacaaagctgacaccgtggcgccgttcgcagcatgccatccgat
ttatcaaaacctgcccggcaccacgcccggaaagttacgtcgaactggataacgcacatcgacttcgctccgaatagcaacaatgcggccattcc
gttatacgtatctcatggatgaaactgtgggtcgataatgacacccgtaccgcagttcctgttaatgtgaacgaccggctgtcgacttc
cgccaccaataatcgccactgccaactcgagcaccaccaccac

695

Expressed amino acid sequence of LCC by *E. coli*

QTNPYARGPNPTAASLEASAGPFTVRSFTVSRPSGYGAGTVYYPTNAGGTVGAIIVPGY
TARQSSIKWWGPRLASHGFVVITIDTNSTFDYPSSRSSQQMAALRQVASLNGDSSSPIYGK
VDTARMGVGMHSMGGGASLRSAANNPSLKAAIPQAPWDSQTNFSSVTVPLIFACENDSI
APVNSHALPIYDSMSRNAKQFLEINGGSHSCANSGNSNQALIGKKGVAWMKRFMDNDTR
YSTFACENPNSTA VSDFRTANCSLEHHHHHH

696

697

698 ICCM

Nucleotide sequence of ICCM without its original signal peptide sequence

atgagcaaccgtaccagcgtggcccgaatccgaccgcagcgactgaccgcagatggccgttagcgtggcaacctacaccgtcac
gcctgtcagtctcggtttggcgggtggcgtgatttattacccgaccggcacgtctgacgttcggtgtggcatcgcgatgagtccgggtatacc
gcagatgctagctctggcatggctgggtcgccgtggctccatggcttgcgtgggtgatataacacgaattcacgtttcattatccgg
acagccgcgcctctcagctgagtgccgcctgaactacctgcgtaccagttccccgagcgcgcgtcgacgtctggatgcaaatcgtctg
gcgggtgccggcatttatgggtggcggtggcaccctgcgtattgcagaacaaaacccgagcctgaaagcggctgtcccgtgacccctg
gcacaccgataaaacgttaataccagtgtcccggtgctgattgtggcgcagaagctgacaccgtggccgggttcgcagcatccatccc
gttttatcaaaacctgcccggcaccacgcccggaaagttacgtcgaactgtgcacgcacattgcgtccgatgagcaacaatgcggccatt
tccgtttatacgatctcatggatgaaactgtgggtcgataatgacacccgttaccgcgcaggctgtgtaatgtgaacgacccggctgtgcgac
ttccgcaccaataatgccactgccaactcgagcaccaccaccaccac

699

Expressed amino acid sequence of LCC by *E. coli*

MSNPYQRGPNPTRSALTADGPFSVATYTVSRLSVSGFGGGVIYYPTGTSLTFGGIAMSPGY
TADASSLAWLGRRFLASHGFVVLVINTNSRFDYPDSRASQLSAALNYLRTSSPSAVRARLD
ANRLAVAGHSMGGGTLRIAEQNPSLKAAVPLTPWHTDKTFNTSVPVLIVGAEADTVAP
VSQHAIPFYQNLPSSTPKVYVELCNASHIAPMSNNAAISVYTISWMKLWVDNDTRYRQFL
CNVNDPALCDFRTNNRHCQLEHHHHHH

700

701

702 **Legends for Supplementary Information Figures**

703 **Supplementary Information Fig. 1 | Schematic diagram of Mutcompute.** **a.** Creating a
704 microenvironment: MutCompute begins by centering itself on the alpha carbon of a particular residue
705 in the protein and filters all peptide atoms within a 20 angstrom cube (the orientation of the cube is
706 normalized with respect to the protein backbone). In the filtering process, we create an artificial, self-
707 supervised label by excluding all atoms that belong the center residue. **b.** Encoding the
708 microenvironment: The filtered atoms are then encoded into a 7-channel voxelated representation with
709 a voxel resolution of 1A³. **c.** Running MutCompute on a Microenvironment: The 7-channel voxelated
710 representation of a microenvironment is then passed to the CNN model, MutCompute. The model can
711 be broken into 2 parts: Feature extraction and classification. The feature extraction portion consist of
712 convolutional and max pooling layers and is then flattened into a 1D-vector before being passed to the
713 classification layers of the model. The output is a probability mass function of the likelihood each of
714 the 20 amino acids was the amino acid in the center of the microenvironment. We do this process for
715 every residue in the protein to identify residues for mutagenesis.

716

717 **Supplementary Information Fig. 2 | Disfavored PETase residues flagged by MutCompute from**
718 **the wild-type and ThermoPETase crystal structures.** MutCompute outputs a probability
719 distribution that describes the likelihood of each of the 20 canonical amino acids to be the wild-type
720 amino acid for the surrounding chemical environment. A disfavored residue is defined as a residue
721 where the amino acid with the highest predicted probability is not the wild-type amino acid. Here, a
722 30% wild-type probability cutoff was used to down select disfavored residues.

723

724 **Supplementary Information Fig. 3a | Predictions (based on wild-type PETase) ranked by fold**
725 **change in the probabilities between the predicted and the wild-type amino acid.** Fold change
726 predictions are provided as a means of down-selecting potential mutations.
727

728 **Supplementary Information Fig. 3b | TOP 10 ranked predictions (based on wild-type PETase).**
729 The top 10 mutations predicted for the wild-type PETase scaffold are presented.
730

731 **Supplementary Information Fig. 3c | Predictions (based on ThermoPETase) ranked by fold**
732 **change in the probabilities between the predicted and the wild-type amino acid.** Fold change
733 predictions are provided as a means of down-selecting potential mutations.
734

735 **Supplementary Information Fig. 3d | TOP 10 ranked predictions (based on ThermoPETase).**
736 The top 10 mutations predicted for the ThermoPETase scaffold are presented.
737

738 **Supplementary Information Fig. 4 | Selecting mutations based on experimental catalytic activity**
739 **measurements.** A scheme for selecting mutations based on experimental evidence is provided.
740

741 **Supplementary Information Fig. 5 | Thermostability of the PETase variants incorporating the**
742 **mutations predicted by Mutcompute and their respective scaffolds—wild-type PETase (WT),**
743 **ThermoPETase (Thermo), DuraPETase (Dura).** The melting temperature of each enzyme was
744 determined by DSC. All measurement were conducted in triplicate (n=3).
745
746

747 **Supplementary Information Fig. 6 | Protein yield of the PETase variants incorporating the**
748 **mutations predicted by Mutcompute and their respective scaffolds—wild-type PETase (WT),**
749 **ThermoPETase (Thermo), DuraPETase (Dura).** Protein yields from *P. putida* purification
750 experiments indicate improved yields from mutant enzymes.

751

752 **Supplementary Information Fig. 7 | The PET-hydrolytic activity of FAST-PETase outperformed**
753 **various PHEs at mild temperatures and modest pH.** Comparison of PET-hydrolytic activity of
754 FAST-PETase, wild-type PETase (WT), ThermoPETase (Thermo), DuraPETase (Dura), LCC and
755 ICCM across a range of pH (6.5 – 8.0) at reaction temperatures of 30 °C (**a.**) and 40 °C (**b.**). PET-
756 hydrolytic activity was evaluated by measuring the amount of PET monomers (the sum of TPA and
757 MHET) released from hydrolyzing gf-PET film by the tested enzymes after 96 hrs of reaction time.
758 All measurement were conducted in triplicate (n=3).

759

760 **Supplementary Information Fig. 8 | Mass, crystallinity %, molecular weights (M_n , M_w),**
761 **polydispersity indices (D) and time for complete degradation of various pc-PET films by FAST-**
762 **PETase.** The circular pc-PET films (6 mm in diameter) were hole-punched from 51 different post-
763 consumer plastic products used in the packaging of food, beverages, medications, office supplies,
764 household goods and cosmetics available at local grocery store chains (Walmart, Costco, and HEB).
765 The pc-PET films were hydrolysed by serial treatment with FAST-PETase at 50 °C until the films were
766 completed degraded. The enzyme solution (200 nM of FAST-PETase in 100mM KH₂PO₄-NaOH (pH
767 8.0) buffer) was replenished every 24 hours. The crystallinity % of the intact pc-PET films was
768 determined by DSC. The initial mass of the films was determined gravimetrically by a digital scale.
769 Both DSC and gravimetric measurements were conducted in triplicate. Means ± s.d. (n=3) are shown.

770

771 **Supplementary Information Fig. 9 | Scatterplot of degradation rate versus (a.) initial mass or (b.)**
772 **crystallinity % or (c.) weight average molecular weight (Mw) or (d.) number average molecular**
773 **weight (Mn) or (e.) polydispersity indices of the hole-punched films from 51 different post-**
774 **consumer plastic products.** Degradation rate was not found to be dependent on any one metric of
775 these various plastics.

776

777 **Supplementary Information Fig. 10 | Time-course of crystallinity % of the degraded pc-PET**
778 **film.** The hole-punched PET films from a bean cake PET container were treated with FAST-PETase
779 for 0 hr, 4hr, 8 hr, 12 hrs 16 hr in 100 mM KH₂PO₄-NaOH (pH 8.0) buffer at 50 °C. Crystallinity % of
780 the films was determined by DSC. All measurement were conducted in duplicate (n=2).

781

782 **Supplementary Information Fig. 11 | Scanning electron microscopic analysis of the pc-PET films.**
783 The hole-punched PET films from a bean cake PET container were treated with FAST-PETase for 0
784 hr, 8 hr, 16 hr in 100 mM KH₂PO₄-NaOH (pH 8.0) buffer at 50 °C.

785

786 **Supplementary Information Fig. 12 | The surface roughness of the pc-PET films determined by**
787 **atomic force microscopy.** The hole-punched PET films from a bean cake PET container were treated
788 with FAST-PETase for 4 hr, 8 hr, 12 hr, 16 hr and 20 hr in 100mM KH₂PO₄-NaOH (pH 8.0) buffer at
789 50 °C. The time-course profile of the surface roughness indicated that longer exposure times with
790 FAST-PETase resulted in higher degree of surface roughness on the pc-PET films. RMS represents
791 root mean square.

792

793 **Supplementary Information Fig. 13 | Time-course of PET-hydrolytic activity of LCC and ICCM**
794 **at reaction temperatures of 55 °C, 60 °C, 65 °C, and 72 °C.** PET-hydrolytic activity was evaluated
795 by measuring the amount of PET monomers (the sum of TPA and MHET) released from hydrolyzing
796 the pc-PET (Bean cake plastic container) film by the tested PHEs at various time points. 100 mM
797 KH₂PO₄-NaOH (pH 8.0) buffer was used for all reactions shown in this figure. All measurement were
798 conducted in triplicate (n=3).

799

800 **Supplementary Information Fig. 14 | A closed-loop PET recycling process.** Demonstration of a
801 closed-loop process for enzymatically degrading and then regenerating PET in the course of several
802 days.

803

804 **Supplementary Information Fig. 15 | a. ¹H NMR (400 MHz, *d*₆-DMSO) spectra of TPA recovered**
805 **from degraded PET solutions.** The peak at 8.029 ppm corresponds to the hydrogen nuclei of the
806 benzene ring. **b. ¹H NMR (400 MHz, CDCl₃) spectra of DMT synthesized from TPA.** The peak at
807 8.081 ppm corresponds to the hydrogen nuclei of the benzene ring. The peak at 3.93 ppm corresponds
808 to the hydrogen nuclei of the methyl group.

809

810 **Supplementary Information Fig. 16 | DSC trace of PET regenerated from the degraded solutions.**
811 The crystallinity of this regenerated PET is 58.46%. The melting onset is 243.6 °C. The melting peak
812 temperature is 258.4 °C. The glass transition temperature is 84.3 °C.

813

814 **Supplementary Information Fig. 17 | X-ray crystal structure of FAST-PETase. a.** Overall crystal
815 structure of FAST-PETase. Catalytic triads (S160, D206, H237) are shown in blue sticks. Mutations

816 originating from ThermoPETase (S121E, D186H, R280A) are shown in pink sticks, and novel
817 mutations predicted by the neural network are shown in green-yellow sticks. **b-c.** 2F_o-F_c map
818 (contoured at 1.5σ) shown as grey mesh superimposed on the stick models of novel mutation sites (b.)
819 R224Q, (c.) N233K.

820

821 **Supplementary Information Fig. 18 | Statistics of the crystal structural determination of FAST-**
822 **PETase.** Information about the obtained crystal structure is provided.

823

824 **Supplementary Information Fig. 19 | Stages of degradation of pc-PET films by FAST-PETase.**
825 **a. The transparent pc-PET film (6 mm in diameter) was completely degraded (only cutting edges**
826 **of the film remained) after 24 hrs of a single treatment with FAST-PETase at 50 °C. b. The**
827 **colored pc-PET film (6 mm in diameter) was completely degraded (only cutting edges of the film**
828 **and some colorants remained) after six day of serial treatment with FAST-PETase at 50 °C.**
829 Enzyme (200 nM) treatment was performed with 100 mM KH₂PO₄-NaOH (pH 8.0) buffer.